Design guidelines for supersonic stators operating with fluids made of complex molecules

Anand, Nitish; Colonna, Piero; Pini, Matteo

DOI
10.1016/j.energy.2020.117698

Publication date
2020

Document Version
Final published version

Published in
Energy

Energy 203 (2020) 117698

Contents lists available at ScienceDirect

Energy

journal homepage: www.elsevier.com/locate/energy

Design guidelines for supersonic stators operating with fluids made of complex molecules

Nitish Anand , Piero Colonna , Matteo Pini *

Propulsion and Power, Delft University of Technology, Kluyverweg 1, Delft, 2629HS, the Netherlands

ARTICLE INFO

Article history:
Received 2 February 2020
Received in revised form
25 March 2020
Accepted 22 April 2020
Available online 10 May 2020

Keywords:
Supersonic vanes design
Computational fluid dynamics
Post-expansion ratio

ABSTRACT

Supersonic stator vanes account for two-thirds of the fluid-dynamic losses in high temperature mini-Organic Rankine Cycle (ORC) turbines. As a result, the overall performance of the turbo-expander mainly depends on the design of the stator. Currently, there is no established correlation for the optimal design of such cascades. This work concerns an investigation about the accuracy of the only design method currently available for the design of supersonic stators operating with fluids made of complex molecules. A physics-based analytical model and a CFD-based model were developed to estimate the optimal post-expansion ratio and to compare their results with the Deych's model. The analysis shows that the Deych's method fails to accurately predict the optimum value of the post-expansion ratio. The study covers also the assessment of the optimum post-expansion ratio in relation to the solidity, the design flow angle and the total-to-static expansion ratio. The outcome demonstrates that there exists a unique optimum post-expansion ratio for a set of primary stator design parameters. In summary, vanes operating with a substance made of complex molecule as the working fluid, which is typical of high-temperature ORC turbines, feature a unique theoretical value of the optimum post-expansion ratio for a given total-to-static expansion ratio. New correlations are required to predict this value.

1. Introduction

The high-expansion ratio is a defining feature of unconventional turbomachinery, i.e., turbomachinery operating with non-conventional working fluids like those treated for example in Ref. [1,2]. Given that such working fluids are made of complex organic molecules for which the speed of sound is quite low, the stator often operates at highly supersonic flow conditions [3,4]. As a result, new and ad hoc fluid dynamic design methods have been developed in recent times.

ORC power systems are becoming increasingly relevant because they can efficiently convert thermal energy from renewable and waste heat sources [3]. Regardless of its extremely wide application range, the full potential of ORC technology is not realized yet. Economic viability will increase if current technical challenges affecting system performance versus cost are overcome. One issue affecting turbine design and performance of high-temperature high-expansion ratio machine is the complex and non-ideal fluid dynamics within the stator [5]. It has been recently shown, see Refs. [6], that the fluid dynamic losses occurring in the stator of an existing high-temperature high-expansion ratio ORC turbine amount to approximately two-thirds of the total losses of the turbine. This is the case in such type of small-capacity turbines, which are always highly loaded in order to limit the number of stages to unity because of economic constraints. Therefore, the design of efficient stator cascades is critical.

The preliminary design of supersonic stationary vanes involves the choice of several parameters, e.g., the flow angle (φ_a), the expansion ratio (β_{t1}), the degree of divergence (DoD), the solidity (σ) etc., based on correlations. The blade profile is then obtained with the Method of Characteristics (MoC) and refined by means of computational fluid dynamics (CFD) simulations [1]. The mechanical verification of the fluid dynamic design completes the design iteration. Recent studies already dealt with the detailed fluid dynamic design of ORC stators [7,8]. However, the optimal choice of preliminary design parameters dictating the subsequent detailed fluid dynamic design phase has not been treated in the literature yet. Currently, therefore, correlations which were developed to obtain preliminary design parameters for conventional gas turbines are adopted, and the optimal design of supersonic ORC blades can

* Corresponding author.
E-mail addresses: n.anand@tudelft.nl (N. Anand), p.colonna@tudelft.nl (P. Colonna), m.pini@tudelft.nl (M. Pini).

https://doi.org/10.1016/j.energy.2020.117698

only be obtained by resorting to computationally expensive numerical optimization based on high-fidelity CFD, and starting from highly suboptimal configurations.

The degree of divergence is the preliminary design parameter that has the largest impact on the resulting fluid dynamic performance of supersonic ORC vanes [8]. To the authors knowledge, the only model that can be currently employed to calculate the optimal degree of divergence is the one proposed by Deych [9]. This model provides an estimate of the optimum degree of nozzle divergence (DoD) as a function of the stator exit Mach number. The model was derived for the case of supersonic axial cascades operating with air as working fluid, therefore its application to the design of ORC stators affected by non-ideal compressible flow effects is arguably unjustifiable from a theoretical point of view. The objectives of the study documented in this paper are (i) to discuss the accuracy and limitations of the Deych's model, henceforth referred to as *empirical method*, if applied to nozzles operating with fluids different than air, and (ii) to assess the variability of the optimal post-expansion ratio with respect to primary design variables, namely, the flow metal angle, the solidity and the expansion ratio.

To achieve these goals, a physics-based and a CFD-based loss estimation models, limited to perfect gas flows, were developed and these are referred to as *analytical method* and *CFD-based method* in the following. The analytical method estimates the boundary-layer and mixing losses for a typical supersonic axial vane configuration. The losses in the boundary-layer are evaluated according to the procedure described in Ref. [10]. The mixing loss is evaluated by applying the mass, momentum and energy conservation equations to the semi-bladed region of the stator vane, as explained in Refs. [11]. The CFD-based method comprises of a detail design procedure and a simulation. The vane geometry generation method is adapted to handle axial configurations from the method described in Ref. [8]. The fluid-dynamic performance of the blades is calculated using the open-source Reynolds averaged Navier Stokes (RANS) solver SU2 [12]. The flow equations are complemented by the one-equation Spalart-Allmaras turbulence model [13].

In order to investigate the accuracy of the empirical model, the optimum DoD (or alternatively, the optimum post-expansion ratio) obtained from this model is compared to the values calculated with the numerical and the analytical methods. Additionally, the analysis is extended to consider working fluids ranging from those made of simple molecules, to those made of complex organic molecules in order to study the effect of the fluid molecular complexity on the optimum post-expansion ratio. The variation of the optimum post-expansion ratio with the primary design variables is assessed by scanning the design space with the CFD-based method.

2. Methodology

The flow domain of a typical axial stator vane can be divided into three sections, see Fig. 1 (a): the converging section between station (t) and (o), the diverging section between station (o) and (a) and the semi-bladed section between station (a) and (1). The assessment of the empirical method is based on the comparison of the optimal DoD calculated with the empirical method with those obtained with the analytical and the CFD-based methods.

2.1. Empirical method

In 1965, Deych illustrated a method to estimate the preliminary DoD for a stator vane operating in transonic/supersonic flow conditions [9]. To date, this is the only method available and adopted in common practice. According to this method, the optimum DoD is defined by the relation

$$\mathrm{DoD}_{\mathrm{empirical}} = \frac{A_\mathrm{a}}{A_\mathrm{o}} = \begin{cases} 1, & \text{for } M_1 \le 1.4, \\ 1 + (0.5M_1 - 0.4)\left[\dfrac{1}{\mathscr{A}_{\mathrm{is}}(M_1,\gamma)} - 1\right], & \text{for } M_1 > 1.4, \end{cases} \tag{1}$$

where, M_1 is the stator design Mach number, A_o is nozzle throat width, A_a is nozzle outlet width, $\mathscr{A}_{\mathrm{is}}$ is the area ratio corresponding to an isentropic expansion and γ is the heat capacity ratio. The current design practice is thus that nozzles for which the design M_1 is lower than 1.4 (transonic) are made without the diverging section, because the semi-bladed section provides the flow with a sufficient degree of expansion without an excessive penalty in terms of efficiency. In contrast, supersonic nozzles ($M_1 > 1.4$) are always designed with a diverging section.

2.2. Analytical method

Two of the major dissipation mechanisms in supersonic axial vanes are due to mixing and viscosity in the boundary layer. The procedure to analytically estimate these losses is as follows:

(a) Mixing losses. The amount of kinetic energy that is dissipated due to mixing is estimated, as described in Ref. [11], by solving the mass, momentum and energy conservation equations in the control volume encompassing the semi-bladed section of the vane, see Fig. 1(a). The flow deviation angle is

$$\Delta\varphi = \arctan\left[\frac{\frac{\gamma}{1-\gamma}\beta_{1\mathrm{a}}\tan\varphi_\mathrm{a} \pm \sqrt{(1-\beta_{1\mathrm{a}})\left(\frac{2\gamma}{\gamma-1}M_\mathrm{a}^2 - 1 - \frac{\gamma+2}{\gamma-1}\beta_{1\mathrm{a}}\right) + \left(\frac{\gamma\beta_{1\mathrm{a}}}{\gamma-1}\tan\varphi_\mathrm{a}\right)^2}}{1 + \gamma M_a^2 - \beta_{1\mathrm{a}}}\right], \tag{2}$$

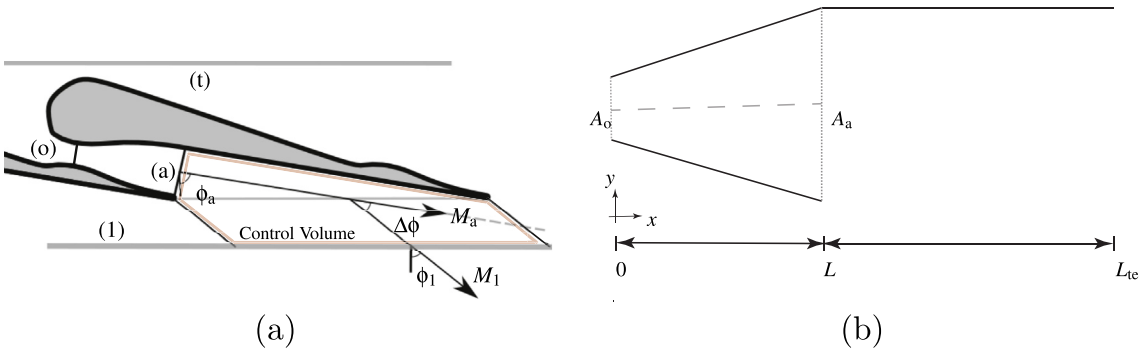

Fig. 1. Schematics of the nozzle geometries related to the analytical loss models: (a) geometry for the mixing loss model, showing Mach number, deviation angle and the different stations in the supersonic vane. The control volume is outlined in red. (b) illustration of the domain considered for the computation of the boundary layer losses. (For interpretation of the references to colour in this figure legend, the reader is referred to the Web version of this article.)

where, M_a is the nozzle Mach number, φ_a is the design flow angle and $\beta_{1a}^{-1} \equiv \beta_{a1}$ is the post-expansion ratio. The only independent quantity in Eqn. (2) is β_{1a} which allows to evaluate M_1 at the exit of the vane. Thus, the amount of kinetic energy that is dissipated due to mixing can be estimated as

$$\xi_{mix} = \frac{h_1 - h_{is,1}}{h_{is,1}}, \tag{3}$$

where, h is enthalpy, and subscript "is" stands for isentropic.

(b) Boundary layer losses. These losses are due to viscous dissipation within the nozzle boundary layer. Assuming turbulent flow on the blade surface, the kinetic energy dissipation can be calculated as

$$\xi_{bl}|_0^X = \frac{\Delta h_{bl}|_0^X}{h_{is,1}}, \tag{4}$$

where,

$$\Delta h_{bl}|_0^X = T_1 \dot{S} = T_1 \frac{C_d \rho_t}{T_t} \int_0^X \frac{\rho_{xt}(M_x)}{T_{xt}(M_x)} M_x^3 c_{xt}^3 dx \tag{5}$$

and

$$h_{is,1} = 0.5 \cdot \dot{m} v_{is,1}^2. \tag{6}$$

In these equations, C_d is the dissipation coefficient, ρ is the density, T is the temperature, S is the entropy, $\dot{m}$ is the mass flow rate, v is the velocity, c is the speed of sound and subscript "xt" stands for isentropic ratio between properties at station "x" and "t". C_d is equal to 0.002 according to Refs. [10].

The only unknown in Eqn. (5) is the property distribution along the surface of the stator, for which the quasi-1D flow approximation is assumed valid. Since the boundary layer losses in the subsonic section are significantly lower than the boundary layer losses in the supersonic section (as boundary layer losses scale with the cube of the Mach number), only the diverging part of the nozzle and the semi-bladed section are modeled for simplicity. In the diverging section of the nozzle the flow accelerates, while in the semi-bladed section the linear suction side surface guides the flow to the outlet, see Fig. 1(a). The Mach number distribution is computed according to the 1D flow approximation by assuming a linear variation from unity at the throat to M_a at the nozzle outlet section, see Fig. 1(b). The suction side is modeled as a flat plate over which the fluid flows at constant Mach number M_a, see Fig. 1(b). Eqn. (5) applied to the geometry depicted in Fig. 1(b) allows to compute the boundary layer loss in the supersonic vane as

$$\xi_{bl} = 2\xi_{bl}|_0^L + \xi_{bl}|_L^{L_{te}}, \tag{7}$$

where, $\xi_{bl}|_0^L$ is the loss due to the nozzle surface and $\xi_{bl}|_L^{L_{te}}$ is the loss due to the linear suction side.

2.3. CFD-based method

The vane geometries with varying DoD are generated and analysed by following a procedure which can be divided into two parts, namely, *geometry generation* and *CFD simulation*. The procedure is similar to that documented in Ref. [8] for radial vanes, however, it differs regarding the way the axial vane geometry is obtained.

2.3.1. Geometry generation

In order to design an axial supersonic stator, the nozzle geometry obtained by applying the MoC [14,15] is adapted to the vane configuration and the geometry of the converging section is generated by means of Non-Uniform Rational Basis Splines (NURBs) [16]. Details of this MoC are provided also in Ref. [8], while the procedure to create the vane geometry starting from the nozzle obtained with the MoC is as follows.

1. *Scaling factor.* With reference to Fig. 2, two points ss_{te} and ss_{te}^*, which are a pitch-distance (p) apart, are placed on the plane where the trailing edge of the stator is to end. Next, point ss_a is obtained by the intersecting the line originating from point ss_{te} at design flow angle φ_a and the line originating from ss_{te}^* at an angle $90^\circ - \varphi_a$. The line ss_a-ss_{te}, see Fig. 2(a) can then be readily drawn. Point ps_a^* is positioned at a distance equal to the prescribed trailing edge thickness (t) from point ss_{te}^* along the line ss_{te}^*-ss_a.

The diverging-nozzle geometry resulting from the application of the MoC is scaled such that the non dimensional width of the throat is unity, thus determining the value of the exit area of the diverging-nozzle $\mathscr{A}_{is}$ as a function of M_a. In order to complete the construction of the diverging part of the nozzle, the outlet cross-section width calculated with the MoC must be made the same as ss_a-ps_a^*, see Fig. 2(c). This is accomplished by means of a scaling factor $\mathscr{S}$ determined by calculating the ratio of the distance between points ss_a and ps_a^* and $\mathscr{A}_{is}$, namely as

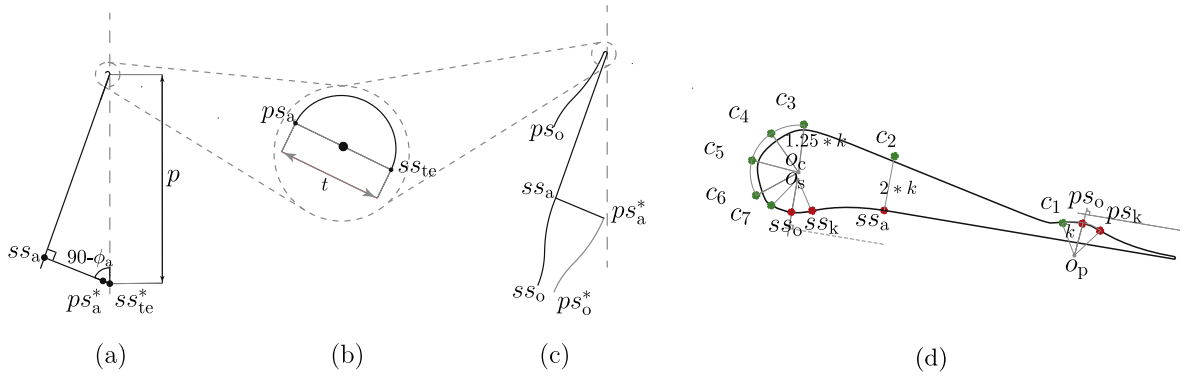

Fig. 2. Schematic representation of the graphic procedure to obtain the geometry of an axial supersonic vane, (a) semi-bladed region, (b) trailing edge (c) diverging-nozzle section and (d) converging section.

$$\mathscr{S} = \frac{l(ss_a, ps^*_a)}{\mathscr{A}_{is}(M_a)}, \tag{8}$$

where, l is the length between ss_a and ps^*_a.

2. *Transformation of the nozzle geometry.* After the nozzle geometry obtained with the MoC is scaled to the factor $\mathscr{S}$, the scaled nozzle is then rotated by an angle φ_a about the center of the throat. The obtained geometry forms therefore the diverging section of the supersonic vane, see Fig. 2(c).
3. *Translation of the pressure side (line ps^*).* In order to obtain a complete blade, thus a continuous line made of the pressure and of the suction side, the pressure side of the nozzle, section ps^* in Fig. 2(c), is translated by a pitch-length to obtain curve ps.
4. *Converging section.* The converging section of the nozzle vane is generated by means of a single NURBs curve connecting the throat points ss_o and ps_o through points c_1-c_7, see Fig. 2(d).

2.3.2. CFD simulation

The performance of the supersonic vanes is computed with the aid of simulations performed with the open-source CFD software tool SU2 [12,17]. The computational domain encompassing one vane geometry is generated using UMG2, an in-house meshing program [18]. An exemplary geometry is depicted in Fig. 3. The computational domain is discretized using clustered quadrilateral elements close to the wall, ensuring a $y^+ < 1$, and triangular elements in the rest of the flow domain. Following from a grid convergence study [19], a mesh of approximately 50,000 elements was chosen as the optimal compromise between accuracy and computational cost. The difference in the value of kinetic energy loss coefficient between the finest mesh and the one selected is 2%. The flow is simulated by solving the RANS equations and the turbulence equations are closed using the one-equation Spalart-Allmaras model [13]. The thermo-physical properties of the fluid are calculated using the polytropic perfect gas model.

The flow simulation is initialized by imposing a uniform state to the fluid everywhere in the domain, with properties corresponding to those of the total conditions at the inlet, and a value of the back pressure at the outlet. In addition, the non-reflective boundary condition, see Refs. [20], is also prescribed. The solution was obtained by using an Euler implicit time-marching scheme with a CFL of 10 while ensuring second-order spatial accuracy. Residual reduction of 4 orders of magnitude was achieved by running the simulations for a maximum of 4000 iterations.

The kinetic energy loss coefficient, accounting for both boundary-layer and mixing losses, is calculated numerically by obtaining mixed-out average quantities at the boundaries, resulting in

$$\xi_{CFD} = \frac{\overline{h}_1 - h_{is,1}}{0.5 \cdot v^2_{is,1}}, \tag{9}$$

where, $\overline{h}_1$ is the averaged enthalpy at the outlet of the stator domain.

3. Case studies

In order to identify the optimum value of the post-expansion ratio β_{a1} ($\beta_{opt,a1}$), the fluid dynamic performance of the vanes with varying β_{a1} is plotted. β_{a1} is varied so as to capture the post-compression ($\beta_{a1} < 1$) and post-expansion ($\beta_{a1} > 1$) phenomena in the semi-bladed section of the stator vane.

The three methods are used to compute $\beta_{opt,a1}$ for nozzles operating with different working fluids. The fluids under investigation range from fluids made of simple molecules to fluids made of

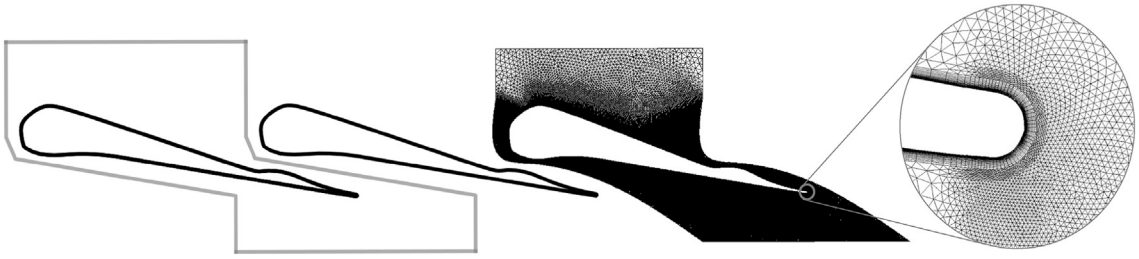

Fig. 3. Representation of the axial vane geometry. The boundary of the computational flow domain is outlined in gray (left). The discretized computational domain is also reported (right), together with the zoomed-in view of the trailing edge.

complex molecules. This wide range of molecular complexity of the working fluids enables to capture the effect of its variation on $\beta_{opt,a1}$. The selected fluids are therefore air, CO_2, toluene and siloxane MM with γ of 1.4, 1.3, 1.055 and 1.025, respectively. The stator design parameters, like, for example, the solidity (σ), the design flow angle (φ_a) and the total-to-static expansion ratio (β_{t1}), are kept constant. The stator vanes are designed for a φ_a of 70°. The solidity of the vane is constrained to unity in all cases. The test vanes are designed to operate with a β_{t1} of 6.0, and with a total temperature and pressure at the inlet of 580 K and 3.2 MPa.

In order to preliminarily assess the variation of $\beta_{opt,a1}$ with the stator design parameters namely, solidity (σ), design flow angle (φ_a) and total-to-static expansion ratio (β_{t1}), vanes operating with toluene were selected. The fluid dynamic performance of the vanes was assessed by using the CFD-based method.

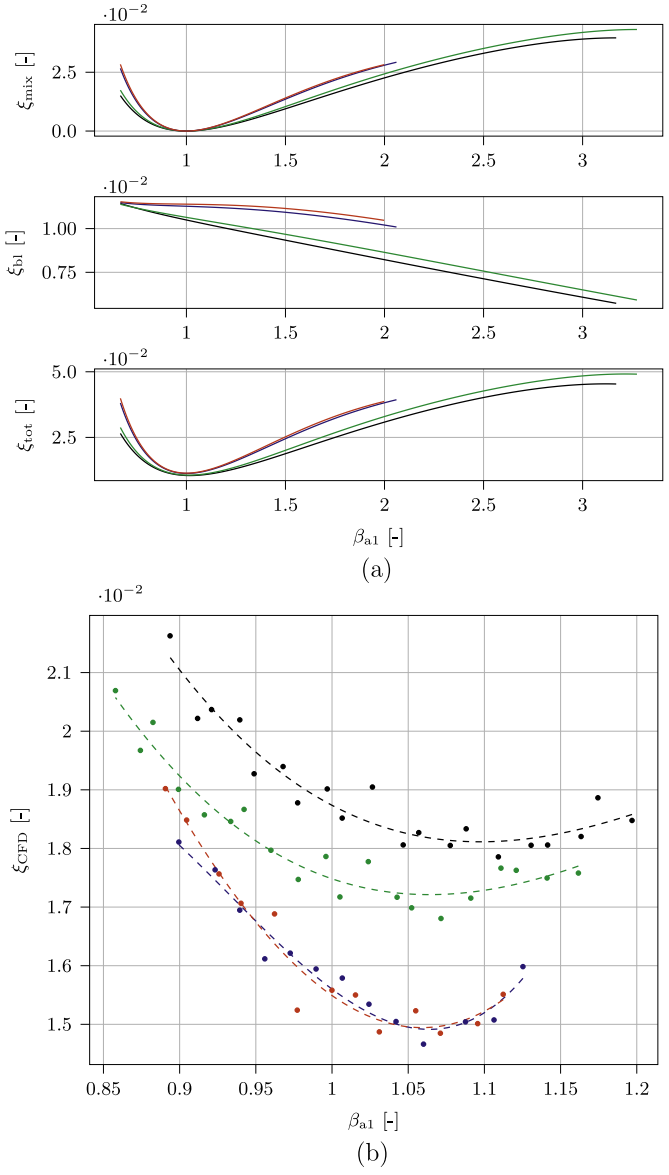

Fig. 4. Variation of ξ with β_{a1} for stator vanes operating with $\beta_{t1} = 6.0$ and $\varphi_a = 70°$ and with air (- - -), CO_2(- - -), toluene (- - -) and MM (- - -) as working fluid. (a) trend lines obtained with the analytical method, (b) trend lines obtained with the CFD-based method. The dots in (b) represent the values obtained from CFD simulations at discrete intervals of β_{a1} and the dashed lines are trend lines obtained by fitting the dots with a cubic functional form.

4. Results

Firstly, the accuracy of the empirical method is documented by means of a comparison of its results with the results of the analytical and the CFD-based methods for the considered working fluids. Next, the variation of $\beta_{opt,a1}$ with design parameters is reported.

4.1. Comparison among the considered methods

The three methods, namely the empirical, the analytical and the CFD-based methods, are employed to calculate the optimum degree of divergence (or alternatively optimum post-expansion ratio) which ensures the least amount of fluid-dynamic losses for the considered test cases.

Fig. 4(a) illustrates the results obtained with the analytical method, that is, the trends of boundary-layer losses, mixing losses and total losses as a function of β_{a1}. As expected, the mixing losses are minimal for $\beta_{a1} = 1$ and the boundary-layer losses increase with the nozzle exit Mach number, i.e., with decreasing β_{a1}. Moreover, the rate of change of the absolute value of the boundary-layer losses is much lower than that of mixing losses. Furthermore, both the boundary-layer and the mixing losses are larger for working fluids made of increasingly complex molecules, possibly because the flow Mach number is increasingly higher for the same operating conditions. The trend of the total loss ξ_{tot}, see Fig. 4(a), suggests that different working fluids imply variations of $\beta_{opt,a1}$ values, which is close to unity in all cases, as mixing-losses dominate the total loss in the stator.

The fluid-dynamic performance of the exemplary vanes are also calculated using the CFD-based method. The σ of the vanes is maintained within 1±0.01 in accordance with the assumption made for the analytical method. Fig. 4(b) reports the estimated vane performance as a function of β_{a1}. The dots represent the values obtained from numerical simulations by linearly varying the DoD while the dashed lines are trends obtained by cubic fitting, in order to identify a value of β_{a1} that can be used for design purposes. The cubic functional form was chosen somewhat arbitrarily after inspection of the trend of the total loss distribution computed with the analytical model.

As opposed to the previous findings, it can be observed that the total loss is inversely proportional to the fluid molecular complexity, i.e., the total loss is higher for flows of fluids made of simpler fluid molecules. This is attributed to shock wave losses and the dissipation due to the impingement of the shock wave on the suction side of the blade. Nonetheless, the increase in total losses from $\beta_{a1} = \beta_{opt,a1}$ to $\beta_{a1} \neq \beta_{opt,a1}$ is higher for fluids made of complex molecules. Finally, Fig. 4(b) shows also that the value of $\beta_{opt,a1}$ is different depending on the working fluid, and it increases with decreasing molecular complexity.

Additionally, it can be observed that the values of ξ_{CFD} is highly sensitive to small changes in the post-expansion ratio β_{a1}, and they become more scattered for β_{a1} away from unity. This is primarily due to the change in the position and strength of the shock wave emerging from the trailing edge of the stator vanes, which plays a key role regarding the adjustment of the flow field with respect to the imposed back pressure. Additionally, the interaction of these shock waves with wake and boundary layer influence substantially the overall performance.

Fig. 5 depicts the Mach number contours for stator vanes operating with toluene as working fluid. The value of β_{t1} is prescribed equal to 6.0, the results of simulations are shown for decreasing β_{a1} (or increasing DoD) from left to right. Fig. 5(b) shows the Mach contour corresponding to the vane with optimal post-expansion ratio. In all cases, a fishtail shock pattern originates at

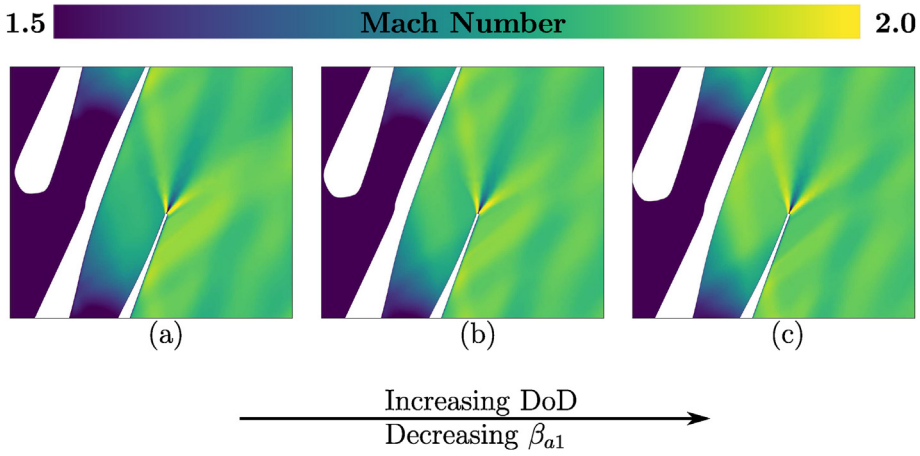

Fig. 5. Mach number contours of vanes operating with Toluene as working fluid for $\beta_{t1} = 6.0$ and $\varphi_a = 71°$. From left to right: (a) $\beta_{a1} > \beta_{opt,a1}$, (b) $\beta_{a1} = \beta_{opt,a1}$ and (c) $\beta_{a1} < \beta_{opt,a1}$.

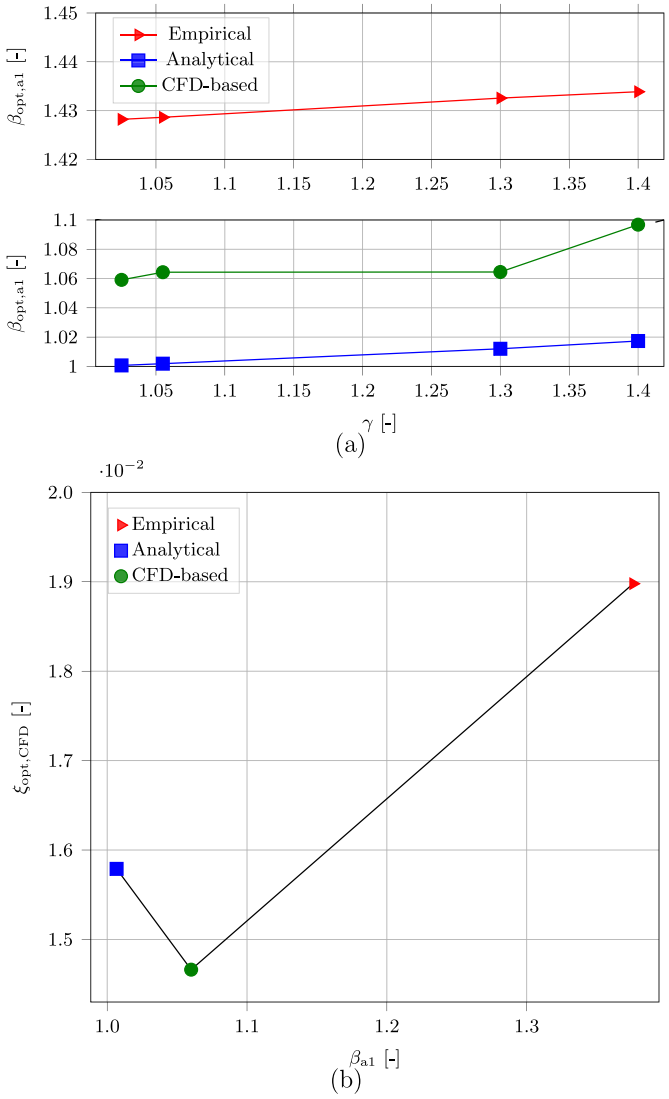

Fig. 6. Comparison of $\beta_{opt,a1}$ obtained with the three design methods (a) Variation of $\beta_{opt,a1}$ depending on the molecular complexity of the working fluid, and (b) ξ_{CFD} obtained by simulating $\beta_{opt,a1}$ from the three methods with Toluene as the working fluid.

the trailing-edge of the vane. It can be seen that the strength of the pressure wave reflecting on the suction side increases with increasing DoD. This is because the flow exiting the nozzle in Fig. 5(c) undergoes a compression ($\beta_{a1} < 1$), while in the case of Fig. 5(a) and (b) the flow further expands ($\beta_{a1} > 1$). The mixing of the two pressure waves downstream eventually dictates the magnitude of the deflection angle and the associated mixing-loss.

The values of $\beta_{opt,a1}$ obtained with the three design methods are plotted against γ in Fig. 6(a), which shows that the trends obtained with the three methods are similar and that flows of fluids made of complex molecules exhibit lower $\beta_{opt,a1}$. Moreover, the value of $\beta_{opt,a1}$ calculated using the empirical method is much higher than the value predicted by the other two methods for all the fluids.

The fluid dynamic performance of the vane operating with toluene at $\beta_{t1} = 6.0$ calculated with the three methods is plotted against β_{a1} in Fig. 6(b). From the outcomes of the analysis, it can be inferred that the use of loss models based on first principles allows one to predict values of post-expansion ratio and total loss in

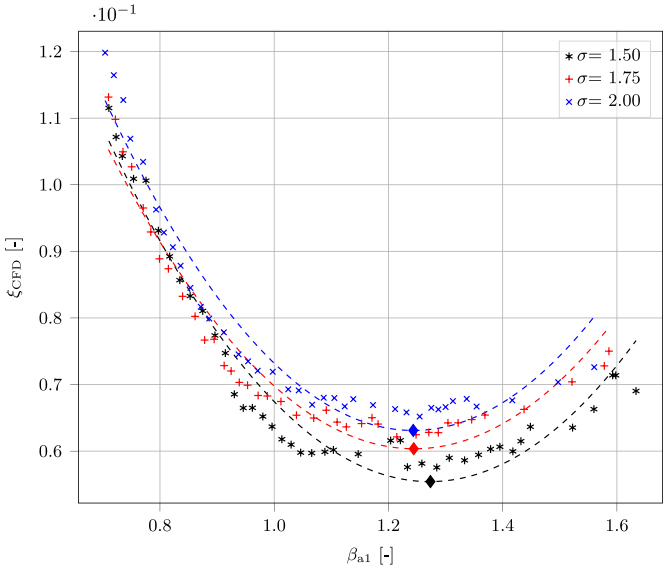

Fig. 7. Variation of ξ_{CFD} with β_{a1} for solidity (σ) of 1.50, 1.75 and 2.0, for $\beta_{t1} = 6$ and $\varphi_a = 71°$. The values corresponding to the scattered points are calculated from the results of CFD simulations, while the dashed lines are the hypothetical trends obtained by cubic fitting. The diamond on the dashed line shows the representation of the estimation of the value of β_{a1} that minimizes ξ_{CFD}.

relatively good agreement with those predicted by more computationally expensive CFD-based methods.

4.2. Variation of the optimal post-expansion ratio ($\beta_{opt,a1}$) with primary design variables

In order to assess the influence of design parameters on $\beta_{opt,a1}$, the vane fluid dynamic performance was assessed with the CFD-based method without constraints on solidity, flow angle and total-to-static expansion ratio. The working fluid selected for this analysis is toluene.

4.2.1. Influence of solidity (σ)

Fig. 7 show the ξ_{CFD} variation related to the considered vanes as a function of β_{a1} for selected solidity values and for prescribed constant values of β_{t1} and φ_a. As expected, the losses in the vanes with higher solidity are higher compared to those with a lower solidity. This is due to the increase in the wetted surface area of the vane with increasing solidity, which increases boundary layer losses. Additionally, it can be observed that $\beta_{opt,a1}$ does not change substantially for different values of solidity. In other words, the solidity parameter should not influence the choice of $\beta_{opt,a1}$ (or DoD) however, for the considered cases, a lower values of solidity entails lower losses.

The Mach number contours of the vanes with varying solidity are illustrated in Fig. 8. The overall flow characteristics, particularly the fish-tail shock pattern and shock wave boundary layer interaction remain identical across the three blades.

4.2.2. Influence of flow angle (φ_a)

In this case, the flow angle is varied while the solidity and β_{t1} are kept constant. Fig. 9 illustrates the variation of ξ_{CFD} with β_{a1} for three values of φ_a.

It can be observed that the losses in the vanes with higher φ_a are higher compared to those of vanes with lower φ_a. The wetted surface area of the bladed region, see Fig. 10, remains the same, and the nozzle geometry is unchanged as the solidity is constrained to a fixed value. However, the length of the straight section connecting the bladed region with the trailing edge increases with the flow angle, i.e., section ss_a-ss_{te} in Fig. 2(c). Consequently, this leads to an increase of boundary layer losses for vanes with higher φ_a. Moreover, the boundary layer blockage effect increases with the increase of the flow angle, thus affecting the resulting boundary-layer and mixing losses. This was confirmed by the computation of the values of entropy production between the sections connecting the adjacent leading edge and the trailing edge of the vanes. These values of entropy production are 4.7, 5.23 and 9.14 J·K^{-1} for φ_a of 71°, 76° and 81°, respectively.

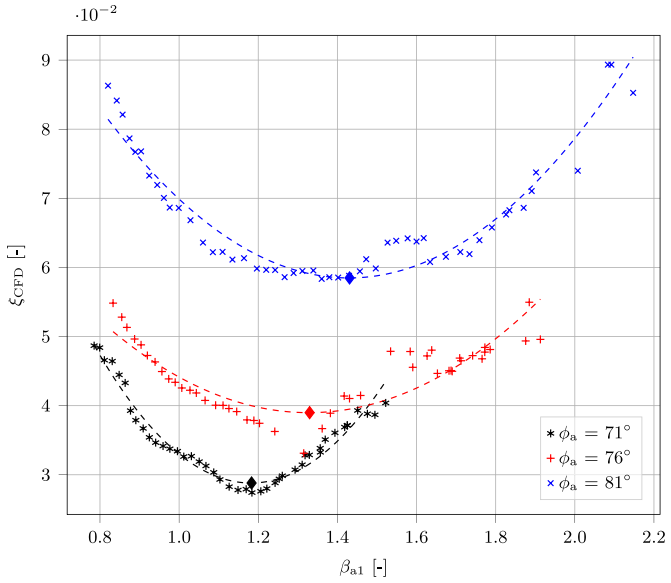

Fig. 9. Variation of ξ_{CFD} with β_{a1} for φ_a of 71°, 76° and 81°. The scattered points represent results from individual CFD simulations while the dashed lines are the hypothetical trends obtained by cubic fitting of these points. The diamonds on the dashed lines highlight the estimation of the optimal value of β_{a1}.

From the results of Fig. 9, it can also be inferred that the optimum post-expansion ratio increases for larger values of flow angles. This is connected to the fact that boundary-layer losses are higher for increasing φ_a, which can become excessively large in case the expansion ratio in the bladed region is kept at comparatively large values. This is due to the expansion ratio in the bladed region being inversely proportional to the post-expansion ratio.

Fig. 10 reports the Mach number contours resulting from the simulation of the optimal vanes for three values of φ_a. It can be seen that the wakes in the vanes with higher φ_a, see Fig. 10(c), are closer to each other compared to those with lower φ_a, see Fig. 10(a), leading to higher mixing losses. Moreover, the trailing edge shock reflects on the suction-side surface more upstream in case of $\varphi_a = 81°$ if compared to the case with $\varphi_a = 71°$, see Fig. 10(a) and (c). This explains the increase in the flow non-uniformity highlighted by the Mach contours from left to right in Fig. 10.

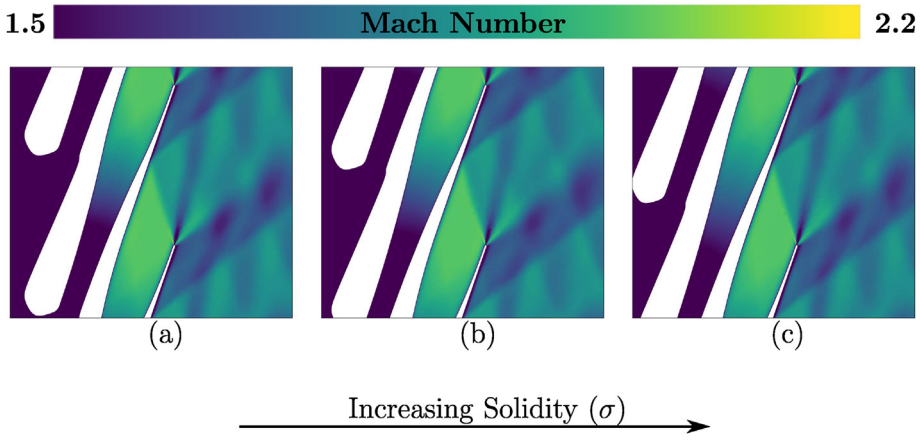

Fig. 8. Mach number contours of vanes operating with Toluene for $\beta_{t1} = 6.0$ and $M_a = 2.0$ with increasing σ from left to right: (a) 1.50, (b) 1.75 and (c) 2.00.

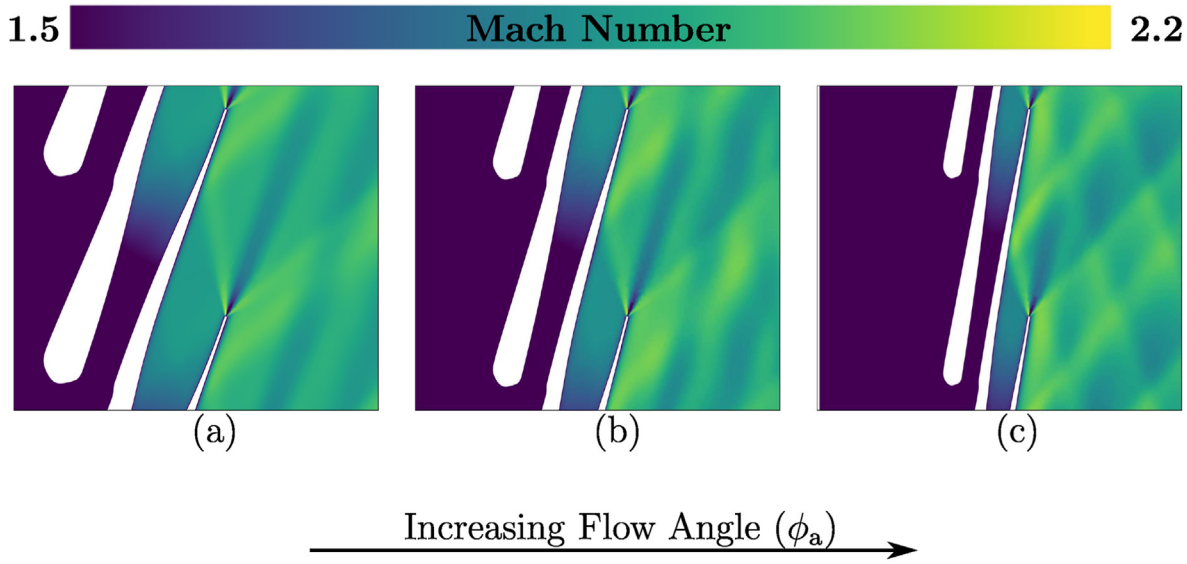

Fig. 10. Mach number contours of vanes operating with Toluene at $\beta_{t1} = 6.0$ and with increasing design flow angle from left to right: (a) 71°, (b) 76° and (c) 81°.

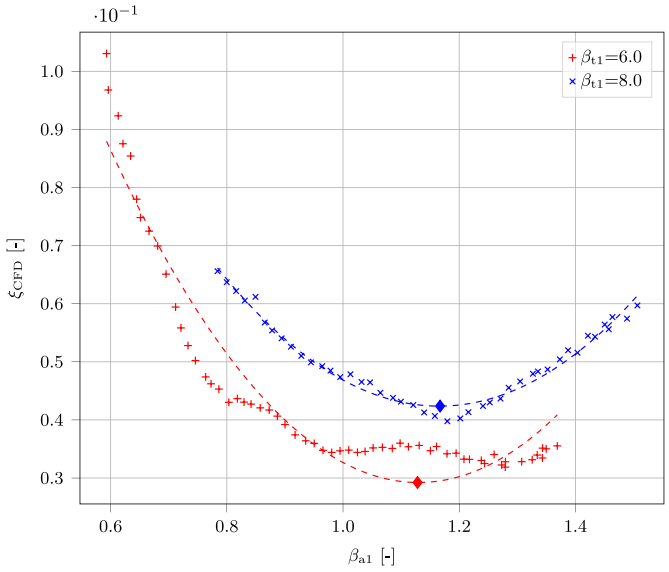

Fig. 11. Variation of ξ_{CFD} with $\beta_{opt,a1}$, for β_{t1} of 6.0 and 8.0. The scattered points represent values computed from CFD simulations while the dashed lines are the hypothetical trends obtained by cubic fitting. The diamonds on the dashed lines highlight the estimation of the optimal value of β_{a1}.

It can thus be concluded that $\beta_{opt,a1}$ is highly sensitive to φ_a.

4.2.3. Influence of total-to-static expansion ratio (β_{t1})

Fig. 11 illustrates the variation of ξ_{CFD} with β_{a1} for two β_{t1} values. It can be seen that the cubic curve fitting is unsatisfactory for $\beta_{t1} = 6.0$. The choice of the cubic functional form for the fitting derived from the results obtained with the analytical method. The high-fidelity CFD simulations can predict more detailed flow features, therefore the resulting trend of the total losses can be different [11].

Additionally, the losses for higher value of β_{t1} are larger, since the Mach number in the flow channel increases with the pressure ratio. Moreover, it can be observed that for $\beta_{t1} = 8.0$ a single value of $\beta_{opt,a1}$ can be identified, while for $\beta_{t1} = 6.0$ the condition of minimum losses is achieved for a range of β_{a1} values. This is possibly a consequence of the stronger shock wave occurring at higher β_{t1} which leads to a higher sensitivity of the overall losses to the post-expansion ratio.

The Mach number contours resulting from the simulation of the optimal vanes for the two values of β_{t1} are illustrated in Fig. 12. The overall flow characteristics, in particular the fishtail shocks and the shock wave boundary layer impingement, are similar despite the different Mach numbers. These results provide a physical justification regarding the reason why higher losses are computed for the vanes illustrated in Fig. 11, where it can be seen that higher losses corresponds to the case with higher β_{t1}.

5. Conclusions

The objective of this work was to investigate the accuracy and thus the suitability of Deych's empirical model for the preliminary design and performance prediction of stator vanes in case the working fluid is made of complex molecules. Deych's method is currently the only one available and adopted in practice for this type of problem. Additionally, the investigation aimed at assessing the influence of primary design variables like, flow angle, expansion ratio and solidity, on the optimum post-expansion ratio of such nozzles.

To this end, the results obtained with the Deych's model were compared with the optimum post-expansion ratio calculated with a physics-based analytical method and that computed with a high-fidelity CFD-based method in some paradigmatic cases. Subsequently, the performance characteristics of a set of stator vanes with varying primary design variables was analysed by means of CFD simulations in order to assess its sensitivity to the degree of post-expansion.

The methods were applied to stator vanes operating with fluids ranging from a fluid made of simple molecules to a fluid made of complex molecules. The following conclusions can be drawn:

1. The optimal performance of axial vanes operating at supersonic flow conditions is characterized by a unique post-expansion ratio which depends on the molecular complexity of the working fluid and on the total to static pressure ratio and design flow angle.

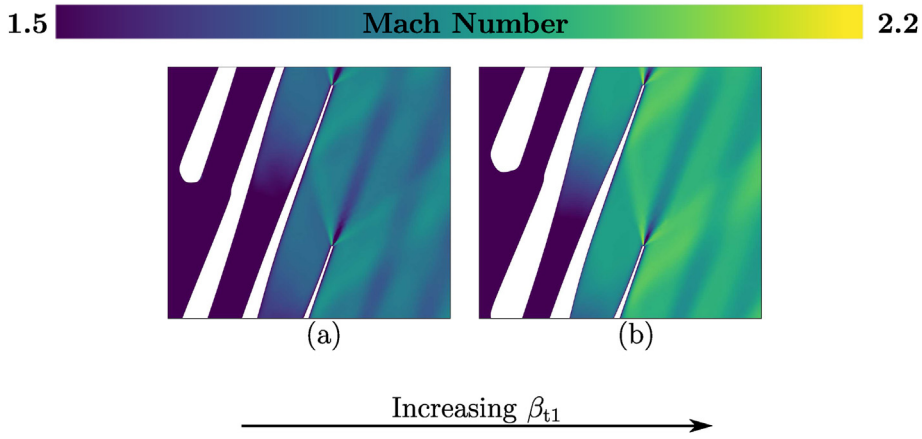

Fig. 12. Mach number contours of vanes operating with Toluene for a $\varphi_a = 71°$ and $\sigma = 1.75$ with increasing β_{t1} from left to right, (a) 6.0, (b) 8.0.

2. The performance calculated with the Deych's method is independent of the design flow angle and the method fails to accurately predict the optimum post-expansion ratio for a vane operating at a total to static pressure ratio of 6.0. Therefore, this method should not be used to design supersonic vanes of ORC turbines. A new method to predict the optimum post-expansion ratio of these vanes should be devised.
3. The analytical method described here, see Sec. 2.2, provides values of the optimal post-expansion ratio well in agreement with those given by the high-fidelity CFD-based method (Sec. 2.3) for the examined fluids and operating conditions. This method provided useful insights into the loss mechanisms affecting the expansion process, which, in turn, allowed to justify the unsuitability of the Deych's method for the design of ORC turbine stators.
4. The blade metal angle is found to be the design variable mostly affecting the optimum post-expansion ratio. The effect of the total-to-static expansion ratio of the cascade on the optimum post-expansion ratio requires further investigation.

Future work will be devoted to the development of simplified analytical models for the prediction of the optimum post-expansion ratio starting from data obtained from CFD simulations to be used in the conceptual design phase of supersonic ORC turbine.

Declaration of competing interest

The authors declare that they have no known competing financial interests or personal relationships that could have appeared to influence the work reported in this paper.

CRediT authorship contribution statement

Nitish Anand: Conceptualization, Methodology, Software, Formal analysis, Writing - original draft. **Piero Colonna:** Supervision, Writing - review & editing. **Matteo Pini:** Conceptualization, Supervision, Writing - original draft.

Acknowledgment

The authors thank the Netherlands Organization for Scientific Research (NWO) which funded this research through the grant with project number 14711.

References

[1] Harinck J, Pasquale D, Pecnik R, van Buijtenen J, Colonna P. Proc IME J Power Energy 2013;227:637–45.
[2] De Servi CM, Burigana M, Pini M, Colonna P. ASME Journal of Engineering in Gas Turbine and Power 2019;141:091021.
[3] Colonna P, Casati E, Trapp C, Mathijssen T, Larjola J, Turunen-Saaresti T, Uusitalo A. J Eng Gas Turbines Power 2015;137.
[4] White M, Sayma A. Appl Energy 2016;183:1227–39.
[5] Colonna P, Harinck J, Rebay S, Guardone A. J Propul Power 2008;24:282–94.
[6] Rinaldi E, Pecnik R, Colonna P. J Turbomach 2016;138.
[7] Guardone A, Spinelli A, Dossena V. J Eng Gas Turbines Power 2013;135.
[8] Anand N, Vitale S, Pini M, Otero GJ, Pecnik R. J Eng Gas Turbines Power 2018;141.
[9] Deych ME, Filippov GA, Lazarev LY. Mashinostroenie Publishing House; 1965.
[10] Denton JD. J Turbomach 1993;115:621–56.
[11] Osnaghi C. Teoria delle turbomacchine, esculapio. second ed. 2013.
[12] Economon DT, Palacios F, Copeland SR, Lukaczyk TW, Alonso JJ. AIAA J 2015;54:828–46.
[13] Spalart PR, Allmaras SR. AIAA J 1992;1:5–21.
[14] Zucrow MJ, Hoffman JD. Gas dynamics volume 1, vol. 1. Limited: John Wiley & Sons Australia; 1976.
[15] Zucrow MJ, Hoffman JD. Gas dynamics volume 2: multidimensional flow, vol. 2. Limited: John Wiley & Sons Australia; 1977.
[16] Piegl L, Tiller W. The NURBS book. second ed. Springer-Verlag Berlin Heidelberg; 1997.
[17] Vitale S, Albring TA, Pini M, Gauger NR, Colonna P. Journal of the Global Power and Propulsion Society 2017;1.
[18] Ghidoni A, Pelizzari E, Rebay S, Selmin V. Int J Numer Methods Fluid 2006;51:1097–115.
[19] ASME 2009. ISBN: 9780791832097.
[20] Giles MB. AIAA J 1990;28:2050–8.